J Mater Sci: Mater Electron (2017) 28:4114–4124
DOI 10.1007/s10854-016-6031-y

CrossMark

Creep behavior of Sn–Bi solder alloys at elevated temperatures studied by nanoindentation

Lu Shen[1,2] · Yuanyuan Wu[2] · Shijie Wang[1] · Zhong Chen[2]

Received: 8 August 2016 / Accepted: 5 November 2016 / Published online: 10 November 2016
© Springer Science+Business Media New York 2016

Abstract The creep mechanisms of eutectic Sn–Bi alloy were evaluated with indentation constant strain rate (CSR) method at elevated temperatures. The activation energy (Q) and creep stress exponent (n) of eutectic Sn–Bi alloy and other alloy compositions were measured in the temperature range from 25 to 100 °C. Prior to this, the indentation CSR testing protocol for evaluation of Q and n was validated through evaluating the pure Sn (grain size >100 μm) at various temperatures. The creep mechanism of large grain-sized Sn was found to be dislocation climb controlled by core diffusion in bulk. Dislocation climb though core diffusion and power-law breakdown were suggested to be the deformation mechanism for pure Bi and Sn–3%Bi alloy, respectively. For the two-phased eutectic Sn–Bi alloy, the creep mechanism was found to be strain rate and temperature dependent. Individual constituent phases were found to take turns to dominate the creep rate at different strain rates.

1 Introduction

Eutectic Sn–Bi solder alloy (58 wt% Bi and 42 wt% of Sn) with melting temperature of 139 °C gains much attention in the microelectronics industry due to the lower processing temperature required. Its good bonding properties with metal bond pad as well as the comparable mechanical properties with traditional SnPb solder make it one of the potential lead-free choices in the market. The mechanical strength and creep properties of eutectic Sn–Bi have been evaluated by the research community with various conventional approaches such as tensile [1–3] and lap-shear tests [4, 5]. The results showed that the alloy had a typical multiple stress-dependent creep mechanism over a wide range of temperature [1, 2, 6]. The major creep mechanisms for metallic materials in medium to high homologous temperature range include dislocation glide, dislocation creep, diffusional creep and grain boundary slipping. Shi et al. [7] established a set of deformation maps based on the stress-sensitive creep behaviour for Sn–Pb eutectic solder. However, such comprehensive deformation maps and life prediction models for lead-free counterparts have yet been fully developed to meet current industrial needs. Studies on creep deformation characteristics on Sn–Ag and Sn–Ag–Cu (SAC) are available in literature [3, 8, 9]. Dislocation climb controlled by lattice diffusion has been postulated as an operative mechanism for SAC. At temperatures close to the melting point of Sn–3.5Ag solder, viscous glide has been proposed as creep mechanism as stress exponent is $\sim$3, and the activation energy is $\sim$30 kJ/mol [8]. Grain boundary sliding (GBS) along Sn–Sn grain boundaries has also been suggested as the operative mechanism for creep deformation in Sn-based alloys. Several diffusion mechanisms have been reported for Sn-based alloys including dislocation core diffusion (Q = 50–70 kJ/mol) or lattice diffusion (Q = 100–120 kJ/mol) over a wide temperature range (25–120 °C).

Existing literatures on the creep mechanism of eutectic Sn–Bi alloy showed large discrepancy in stress exponents

✉ Zhong Chen
ASZChen@ntu.edu.sg

[1] Institute of Materials Research and Engineering, A*STAR (Agency for ScienceTechnology and Research), 3 Research Link, Singapore 117602, Singapore

[2] School of Materials Science and Engineering, Nanyang Technological University, Nanyang Avenue, Singapore 639798, Singapore

and activation energies measured from different groups. For example, Reynold [10] and Morris et al. [5, 11] reported the stress exponent of 11 and the activation energy fell in the range between 83 and 91 kJ/mol, indicating a power-law creep behaviour. However, other groups [2, 12] reported that the activation energy was approximately 60 kJ/mol. They suggested that the creep deformation was mainly accommodated by Bi phase as the similar activation energies were identified for Sn–Bi and pure Bi. One of the possible causes attributing to the large variation in the reported values is the absence of the detailed microstructural information of the alloys under evaluation. It is believed that the microstructure evolution in multi-phased alloys could be a significant factor leading to different deformation mechanisms, particularly when the experiment is conducted at an elevated temperature for a prolonged period of time. Ideally, the microstructure of the Sn–Bi alloys at different heating stages has to be examined in order to understand the impact of the microstructure change to the creep mechanism of the studied alloy.

In this study, we used nanoindentation technique to evaluate the creep behaviour of the Sn–Bi alloy as this technique has shown an indispensable value in evaluating the mechanical properties of small structures especially in sub-micron regime. Not only thin films, but also composite or blend structures, such as the individual phases formed in the blends or multi-phased materials, can be studied once a proper indentation creep testing protocol is established.

The present work was carried out in a nanoindenter with a hearting setup to work at elevated-temperatures. It represents an extended work from our previous publications [13–16] on the creep study of Sn–Bi alloys using nanoindentation at room temperature. The creep properties are evaluated by nanoindentation using the constant strain rate (CSR) method, in which the rate of strain is kept constant throughout the loading process. The volume of the material involved in deformation expands at relatively high rate. Both hardening and recovering processes are radiating outwards from the deformation core at constant rates, making it possible to achieve a steady state during the loading process. In our previous published work [14], we have shown that, under the CSR deformation process, the responding stress is able to achieve a steady stress state after certain depth. Thus, both stress and strain rate are constant representing a steady-state deformation. The detailed discussion of the achievability of steady state with the CRS test and the critical comparison with other indentation methods are available in [13]. In the present study, the creep mechanisms of Sn–Bi alloy were deduced from the creep stress exponent, *n*, and the activation energy, *Q*, obtained at various combinations of external conditions including temperature and strain rate using the CRS test method.

2 Theory

2.1 Nanoindentation creep test

Two different methods are often adopted when nanoindentation is used for creep study: one is the constant load hold test, in which the indenter is pressed into the material at a relatively fast loading rate and is then held at the maximum load for prolonged period of time. Some methodologies were developed based on the assumption that the steady state deformation is achievable during this constant load hold process. The very assumption was used in the work of Marques et al. [9], where they highlighted the indentation data is not interchangeable with the bulk uni-axial creep data due to the progressive change of the contact area between the indenter and the deformed material. This mismatch was addressed by deploying a scaling factor to the finite element model from which satisfied simulation results were obtained. The same method was used in Dean et al. [17] in their study, where the authors also pointed out that in addition to the non-uniformity of the deformation area under the indenter, creep parameters extracted from the secondary indentation creep process are also strongly affected by the primary creep process. A comprehensive finite element analysis model representing the complete deformation process comprising primary and secondary creep was found to be able to generate more accurate creep parameters.

The second indentation method used for creep characterization is CSR test, which was first used by Lucas et al. [18] to assess creep properties of Indium. We have made detailed comparison of the two methods [13]. Comparing to the constant load hold test, genuine steady-state is achievable from the CSR test after the initial transient stage of deformation under CSR condition. Therefore in the present study, CSR test was used for the creep properties evaluation of the Sn and Sn–Bi alloys. In an indentation CSR test, the indenter descending rate in the material is controlled at a CSR until the maximum load is achieved. The strain rate, $\dot{\varepsilon}_i$, is defined as the instantaneous indenter descending rate, *dh*/*dt*, divided by the instantaneous displacement, *h*:

$$\dot{\varepsilon}_i = k_1 \cdot \left(\frac{dh}{dt}\right) \cdot \left(\frac{1}{h}\right) \quad (1)$$

where k_1 is a constant [18]. While the material deforming at prescribed strain rate, the corresponding stress incurred by the material is recorded. The stress (σ), by definition, is the indentation hardness measured in the course of loading process as shown in Eq. (2) [18, 19]:

$$\sigma = H = \frac{P}{A_c} \quad (2)$$

where P is the applied load and A_c is projected contact area. When the stress becomes constant under a CSR condition, the creep reaches a steady-state stage where strain rate and stress follow an exponential relationship as described in

$$\dot{\varepsilon}_i = A_0\sigma^n \exp\left(-\frac{Q}{RT}\right) \quad (3)$$

where A_0 is a material constant, Q is activation energy for the creep deformation, R is the gas constant with a value of 8.314 J/mol K, T is the temperature in absolute scale. n is the creep stress exponent which can be evaluated as the slope of the linear progression of stress and strain rate in logarithm scale at any one temperature:

$$n = \frac{\partial(ln\dot{\varepsilon}_i)}{\partial(ln\sigma)} \quad (4)$$

2.2 Activation energy evaluated by nanoindentation technique

Re-write Eq. (3), strain rate and stress can be expressed in logarithm form:

$$ln\sigma = \left(\frac{Q}{nR}\right)\cdot\left(\frac{1}{T}\right) + \frac{1}{n}(ln\dot{\varepsilon}_i - lnA_0) \quad (5)$$

In an indentation CSR test, strain rate, $\dot{\varepsilon}_i$, is the controllable parameter which is set to be constant throughout the experiment. By plotting $ln(\sigma)$ versus $1/T$, the activation energy Q, which is closely related to the creep deformation mechanism, can be calculated based on the slope of the linear curve.

3 Experimental

3.1 Materials and sample preparation

Polycrystalline Sn and Bi (with average grain size of 317 and 111 μm, respectively, purity >99.99%) were obtained from Sigma-Aldrich©. Sn–3wt%Bi alloy were prepared by mixing the two types of metal chunks at a weight ratio of Sn:Bi = 97:3. Small amount of anti-oxidation solder flux was pre-mixed with the two metals before heating up to 300 °C and kept for 1 h under N_2 atmosphere. The final sample is single phase with averaged grain size of 9 μm. To prepare eutectic Sn–Bi alloy, 50 mg eutectic Sn–Bi solder paste (ESL Europe®) was heated at 150 °C for 1 h before oven cooling. Solidified alloy beads with diameter around 4 mm were formed for the following experiments. Under equilibrium condition, the phase composition of Sn and Bi alloy is governed by their eutectic phase diagram. The two constituents are a pure Bi phase (i.e., Sn has zero solubility in Bi matrix) and a Sn-rich phase (i.e., some Bi is dissolved in Sn matrix). The solubility of Bi in the Sn-rich phase changes with temperature; at 25 °C the Bi concentration is about 3 wt%. Unlike other Sn-based solders, there is no intermetallic compound between Sn and Bi.

3.2 Microstructural study on eutectic Sn–Bi alloy

The eutectic Sn–Bi alloys were annealed at four temperatures (50, 75, 100 and 125 °C) with various durations (10 min, 30 min, 1 h, 2 h, and 4 h) before microstructural examination by scanning electron microscopy (SEM). The cross-section of Sn–Bi samples were grounded and polished to achieve a mirror finish. The SEM images obtained on the flat surfaces of each eutectic Sn–Bi sample were used to calculate the inter-phase spacing (IPS). Samples of two extreme grain sizes, obtained by quenching and by thermal annealed at 125 °C for 30 days, were also prepared for comparison.

3.3 Indentation constant strain rate (CSR) test

The indentation tests were performed on an Agilent G200 Nanoindenter system (TN, USA) with a sharp Berkovich tip. The indenter used in current study has a radius about 50 nm at the apex. The temperature of the sample was controlled through a heating element mounted underneath the holder plate on top of the micrometric tables. The accuracy of the heater temperature control is within ±0.1 °C. After the flat surface was prepared by polishing, CSR indentation tests were conducted on pure Sn, pure Bi, eutectic Sn–Bi and Sn–3wt%Bi samples. Each indentation was made at a prescribed CSR up to a peak displacement of 4000 nm. The edge of the projection area of an indent on sample surface is approximately 28 μm. The depth ramp was immediately followed by a short hold period of 10 s before unloading. Six strain rates (0.01, 0.02, 0.05, 0.1, 0.2, 0.5 s^{-1}) were applied on the material to obtain the corresponding steady-state stress. The stress exponent, n, was obtained using Eq. (4). Five indents were made at every strain rate to ensure the consistency of the generated data. Same set of CRS tests were conducted at a minimum of 3 temperatures for the calculation of activation energy for each material. The testing temperatures selected for Bi and Sn–3%Bi alloy are 25, 50 and 75 °C. To compare the results of Sn with the ones obtained from literature, an additional temperature, 100 °C, was used. For eutectic Sn–Bi alloy, due to the appearance of a slope transition in the strain rate–stress curve at low temperatures, one more temperature at 35 °C was used to assess its transition behaviour.

4 Results

4.1 Microstructural evolution of eutectic Sn–Bi at elevated temperatures

The microstructure images of eutectic Sn–Bi at two extreme cooling conditions, i.e., As-quenched and annealed at 125 °C for 30 days, are shown in Fig. 1a, b. As-quenched sample (Fig. 1a) shows a typical lamella structure with the two constituent phases interlocking each other. For the annealed sample (125 °C for 30 days) in Fig. 1b, coarsening effect on both constituent phases is clearly observed. In addition, the Bi phase has been spheroidized.

To identify the effect of heating on microstructure change, especially within the indentation experimental conditions, the IPS data of the eutectic Sn–Bi alloy was recorded at various annealing time intervals and are listed in Table 1. Only a very small increment in IPS was found under the current experimental conditions, which has no single test exceeding 4 h. The IPS lies between 2.6 and 2.7 µm with the maximum difference of 5.7%. Figure 2a–d illustrate the insignificant changes of microstructure in the current testing conditions. Hence, the impact of the microstructure change during test duration can be ignored in the current experiment.

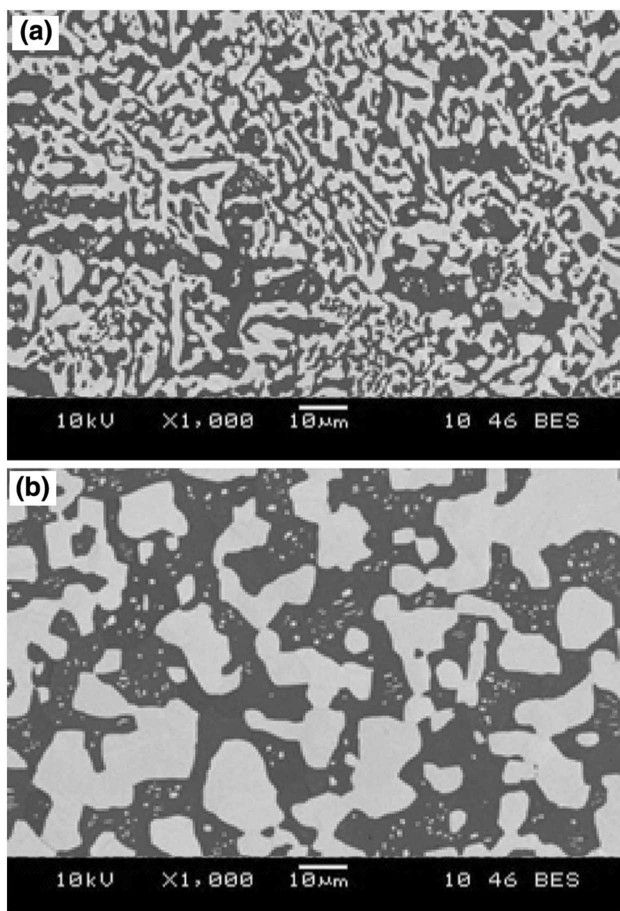

Fig. 1 Microstructures of eutectic Sn–Bi under magnification of ×1000 at two extreme conditions: **a** As-quenched; and **b** annealed at 125 °C for 30 day

4.2 Stress exponent (n) and activation energy (Q)

4.2.1 Pure Sn

Pure Sn with large grain size of 317 µm was evaluated by indentation CSR tests at temperatures ranging from 25 to 100 °C. Each indentation was made at the central location of a grain and the reported value represents an average of five crystal grains at each strain rate. Figure 3 shows the strain rate–stress curves obtained at the four temperatures. Single gradient is observed in all temperatures and the corresponding n values are found to be 7.61–10.09. The values of n are listed in Table 2. Referring to Eq. (5), activation energy (Q) is obtained by multiplying the slope of the $ln(\sigma)$–$(1/T)$ curve with nR, in which n is taken from the average values measured in the temperature range studied.

Figure 4 plots the stress variation with $1/T$ at different strain rates. The slopes of the curves were obtained by linear fit of the experimental data collected at the same strain rate. It is noticed that the data points are supposed to follow a linear trend, however, there was certain degree of deviation from the expected linearity for data points measured for strain rates below 0.5 1/s. We are not able to offer a convincing explanation at this point, one possible reason could be due to choice of crystal grains used in the experiment. Deviation in grain orientation and indentation location (with respect to the grain boundary) is expected between different indentation locations. These experimental uncertainties are going to affect the accuracy of in the obtained creep data. However since the activation energy data are obtained over multiple samples (or locations) with different temperatures, the averaging effect should provide some confidence in their reliability.

The slopes were found to be close to each other in the strain rate range of interest. The average value, 660.6 K, was used in the calculation of the activation energy:

$$Q_{(Sn)} = 8.9 * R * 660.6 = 48.8\,\text{kJ/mol}$$

Table 3 lists n and Q values of single crystal and polycrystalline Sn obtained from various studies. The measured activation energy from this study is in between the literature values of single crystal Sn, i.e., 34–42 kJ/mol [20], and those of the polycrystalline Sn, i.e., 60–88 kJ/mol [3, 21]. However, one should be cautious when comparing the data obtained by nanoindentation and the ones by conventional bulk creep test. A discussion on this matter is

Table 1 The averaged interphase spacing for eutectic Sn–Bi solder alloy annealed at various annealing conditions

Annealing duration	Temperature			
	50 °C (μm)	75 °C (μm)	100 °C (μm)	125 °C (μm)
10 min	2.58	2.60	2.64	2.65
30 min	2.61	2.63	2.62	2.67
1 h	2.57	2.63	2.67	2.67
2 h	2.67	2.68	2.66	2.67
4 h	2.64	2.64	2.71	2.72

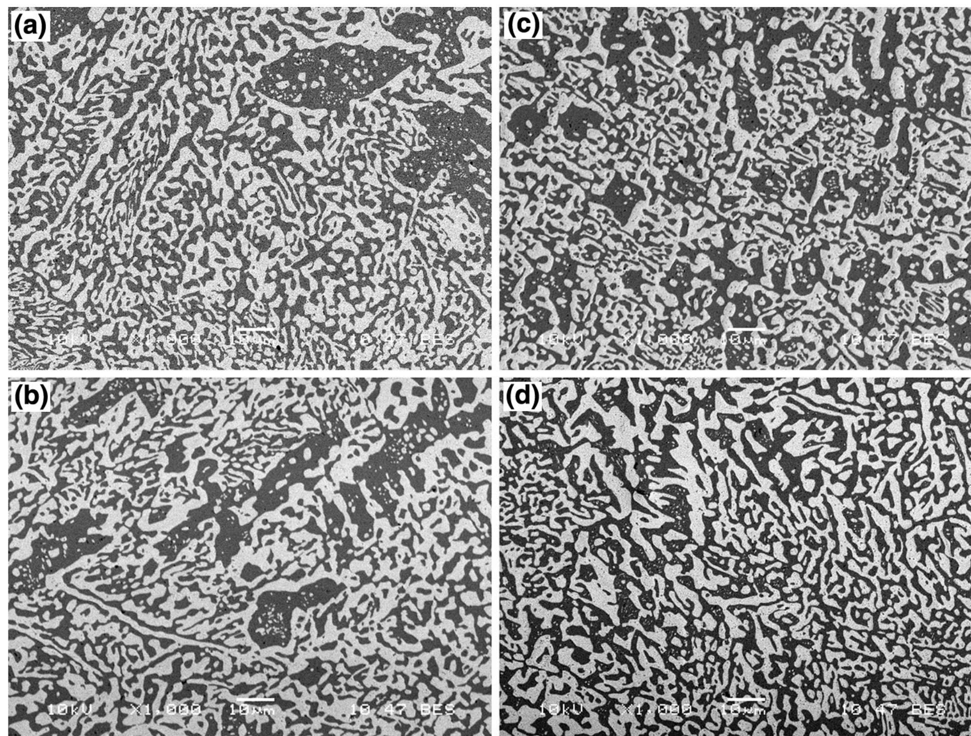

Fig. 2 Microstructures of eutectic Sn–Bi alloy annealed at **a** 50 °C for 10 min, **b** 75 °C for 30 min, **c** 100 °C for 1 h, **d** 125 °C for 4 h, under magnification of ×1000

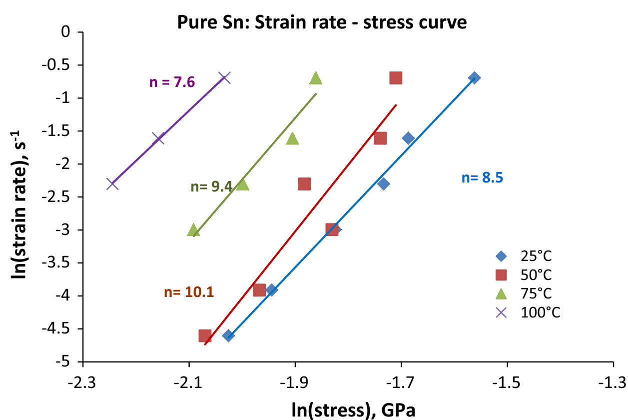

Fig. 3 Strain rate–stress curves for pure Sn measured at four temperatures. Discrete points are the experimental results and the *continuous lines* are the linear curve fitting. Stress exponents are shown as gradient of the curves

made latter on the validity for such a comparison and usefulness of the data obtained by nanoindentation method.

Based on the measured Sn creep properties, Mitlin et al. [6] categorized the creep rate-controlling mechanisms of Sn into high temperature behaviour (T > 150 °C) and low temperature behaviour (T < 120 °C) according to the activation energy obtained at different temperature ranges. The *high temperature creep* of Sn is realized by dislocation climb controlled by diffusion in lattice (i.e., lattice diffusion) with activation energy close to self-diffusion energy of Sn, i.e., 105–109 kJ/mol [6]. The *low temperature creep* of Sn is realized by dislocation climb controlled by core diffusion process [6] with the activation energy typically falls in the range of 30–70% of the self-diffusion energy. In our study, the activation energy of Sn was found to be 48.8 kJ/mol, which is approximately half of the energy for self-diffusion of bulk Sn. Together with the stress exponent

Table 2 Summary of stress exponents of pure Sn, Bi, Sn–3%Bi solid solution and eutectic Sn–Bi solder alloy measured by CSR indentation tests at different temperatures

	Temperatures					Average
	25 °C	35 °C	50 °C	75 °C	100 °C	
Sn	8.5	–	10.1	9.4	7.6	8.9
Bi	10.1	–	7.9	7.0	–	8.4
Sn–3%Bi	11.7	–	12.6	4.8	–	12.2 (50 °C and below)
Eutectic Sn–Bi ($\dot{\varepsilon} = 0.2$–$0.5\ s^{-1}$)	10.3	15.3	–	–	–	12.8
Eutectic Sn–Bi ($\dot{\varepsilon} = 0.01$–$0.2\ s^{-1}$)	6.0	6.5	5.8	4.7	–	5.7

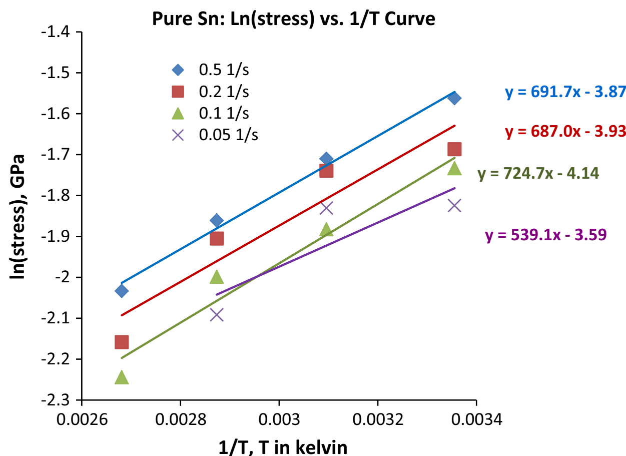

Fig. 4 Ln(stress) versus (1/T) curves for pure Sn

of 8.9, it is reasonable to believe that the creep of pure Sn in the current work behaves as *low temperature creep* controlled by dislocation climb through core diffusion. The creep mechanisms for Sn and all other materials evaluated in this study are summarised in Table 4. The determined creep mechanisms correspond well to the literature findings. Hence, the indentation CSR approach for the creep mechanism evaluation has been validated.

4.2.2 Pure Bi

Figure 5 shows the strain rate–stress curves for pure Bi sample at 25, 50 and 75 °C. Similar to the Sn sample, indentation was made at the centre of each grain. The stress exponents measured from *strain rate–stress* curves are included in Table 2. The values of stress exponents fall in the range of 7.0–10.1 and the average value, 8.4, was used to calculate the activation energy, Q. Figure 6 shows the stress response measured at five strain rates at the three temperatures. The slopes of the curve at each strain rate are close to each other and the average value of 629.4 K was used to calculate activation energy of pure Bi:

$$Q_{(Bi)} = 8.4 * R * 629.4 = 43.7\,\text{kJ/mol}$$

Due to limited number of grains chosen for the creep study, the results on pure Bi obtained in this study may not be used for a direct comparison with the polycrystalline bulk Bi. A discussion regarding this point will be made in the end after all materials systems have been studied. Comparing the activation energy of Bi with the self-diffusion energy of pure Bi (63.5 kJ/mol [22]), the activation energy measured in the current temperature range falls in the *Low-Temperature Creep* range [23, 24] in which the activation energy is lower than self-diffusion energy but the stress exponent is at the higher end of power-law creep range. Based on the experimental data, the creep mechanism of pure Bi is suggested to be dislocation climb with creep rate controlled by core diffusion. The findings are summarized in Table 4.

4.2.3 Sn–3%Bi

The strain rate–stress relationship of Sn–3%Bi solid solution at three different temperatures are shown in Fig. 7. Similar to pure Sn and Bi samples, only one slope is shown in the curves of this single-phased alloy. However, the slope of the curve varies at different temperatures. At lower temperatures (25 and 50 °C), the stress exponents are in the range of 11.7–12.6 (Table 2). While at a higher

Table 3 Literature data for the stress exponent (n) and activation energy (Q) of Sn

Material	Microstructure	Method	Temp (°C)	Stress range (MPa)	Stain rate range (s^{-1})	n	Q (kJ/mol)
Sn [21]	Polycrystalline	Tensile creep	20–225	–	–	–	88
Sn [26]	Polycrystalline	Indentation CLH	25	40–250	10^{-5}–2×10^{-2}	6.7–8.1	–
Sn [3]	Polycrystalline	Tensile creep	23–200	1–30	–	7.6	60
Sn [27]	Polycrystalline	Indentation CLH	25	70–200	3×10^{-5}–10^{-1}	6.3	–
Sn [20]	Single crystal	Impression test	<100	7–50	–	5.0	34–42

Table 4 Summary of stress exponents, activation energies measured from indentation CSR test and self-diffusion energies for pure Sn, Bi and Sn–3%Bi, and eutectic Sn–Bi alloys

Materials	n	Q (kJ/mol)	Q_{SD} (kJ/mol)	Creep mechanism
Pure Sn	8.9	48.8	105–109 [6, 28]	*Low temperature creep.* Dislocation climb controlled by core diffusion
Pure Bi	8.4	43.7	63.5 [22]	*Low temperature creep.* Dislocation climb controlled by core diffusion
Sn–3%Bi (except 75 °C)	12.2	117.9	–	*Power-law breakdown.* GBS as complimentary mechanism
Eutectic Sn–Bi (high $\dot{\varepsilon}$, low T)	12.8	48.2	–	*Low temperature creep.* Dislocation climb by core diffusion in Sn-rich phase
Eutectic Sn–Bi (low $\dot{\varepsilon}$)	5.2–5.7	55.6	–	*Low temperature creep.* Dislocation climb by core diffusion in both constituent phases

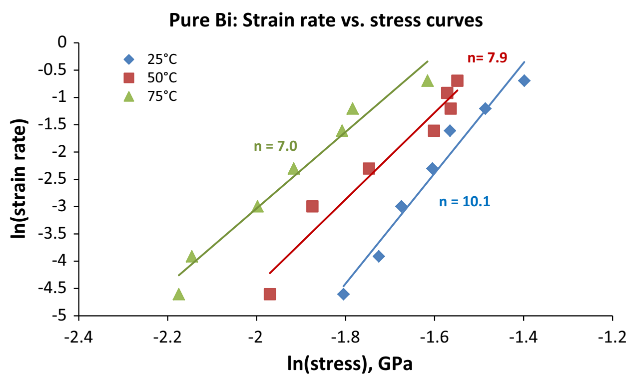

Fig. 5 Strain rate–stress curves for pure Bi measured at different temperatures

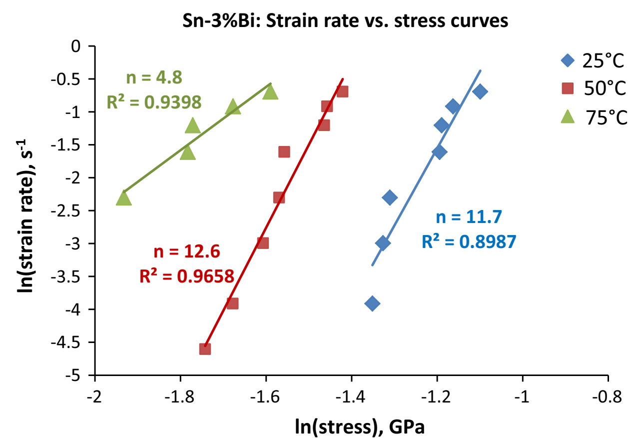

Fig. 7 Strain rate–stress curves for Sn–3%Bi measured at different temperatures

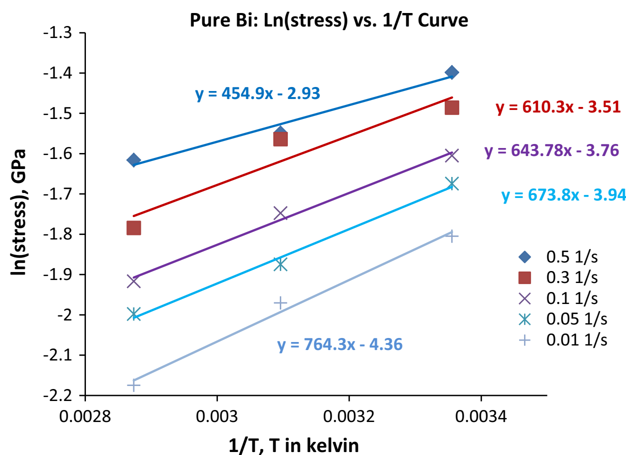

Fig. 6 Ln(stress) versus (1/T) curves for pure Bi

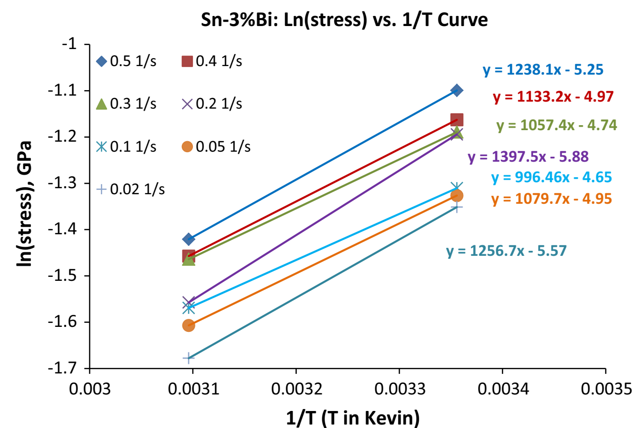

Fig. 8 Ln(stress) versus (1/T) curves for Sn–3%Bi

temperature (75 °C), the slope of the curve dramatically decreases to 4.8, indicating a different mechanism emerged to dominate the creep deformation rate at this temperature range. Figure 8 shows the ln(σ) versus (*1/T*) plot for the two lower temperature deformation process. Similar slopes are found at different strain rates. The average value of 1165.6 K was used to calculate the activation energy of this alloy at temperature range of 25–50 °C:

$$Q_{(Sn-3\%Bi)} = 12.2 * R * 1165.6 = 117.9\,\mathrm{kJ/mol}$$

It is known that the creep behaviour of a solid solution material, such as Sn–3%Bi, could follow either alloys or pure metals. For creep of an alloy, the deformation rate and stress normally follows a power-law relation with *n* value approximately equal to 3, where the creep rate is determined by the rate of dislocation glide [6, 24]. In this type of creep, the solute atmospheres segregate around the dislocations and impede their rate of glide. However, this type of creep requires a slower diffusivity of the solute atmosphere than the self-diffusion rate of the base metal. Mitlin et al. [6] demonstrated that it was impossible to have this type of creep mechanism in operation for Sn–Bi solid solution as Bi had much higher diffusivity in Sn ($D_0 = 72.0\ cm^2/s$) than Sn self-diffusion (7.7–21.0 cm^2/s, depending on temperature and diffusion orientation). On the other hand, creep rate of pure metal is typically determined by one or more types of mechanisms, namely power-law behaviour with stress exponent in the range of 5–10, Harper–Dorn creep with stress exponent of 1, and/or power-law breakdown (PLB) deformation with stress exponent higher than 10. The deformation process in the PLB is controlled by dislocation glide-controlled flow, and the obtained activation energy using Eq. (5) is typically found to be higher than that of the self-diffusion [24]. Comparing to the activation energy of Sn–3%Bi measured in this study, it is noted that the activation energy is close to but slightly higher than the self-diffusion energy of pure Sn. Combining the high stress exponent, high activation energy, and the drastic grain boundary siding observed around indentation mark (refer to Fig. 8a of our previous publication [14]), PLB is thus suggested to be the dominant deformation mechanism for Sn–3%Bi at temperatures below 50 °C.

4.2.4 *Eutectic Sn–Bi alloy*

Figure 9 shows the strain rate–stress relationship of eutectic Sn–Bi alloy at temperatures ranging from 25 to 75 °C. The data at low strain rates and high temperature (75 °C) are not presented due to inconsistency of the result obtained possibly due to the high thermal drift rate at elevated temperatures. At lower temperatures (25 and 35 °C), the alloy exhibits two linear regions on each strain rate–stress curve; while at higher temperatures (50 and 75 °C), only one slope is shown on the strain-rate–stress curve at each temperature. The creep stress exponents, *n*, are summarized in Table 2. It is noticed that *n* values of the Sn–Bi alloy generally fall into two categories: one is around 12.8 as those obtained at higher strain rate range (0.2–0.5 s^{-1}) and lower temperature ranges; another one is around 5.7 as shown in intermediate strain rates

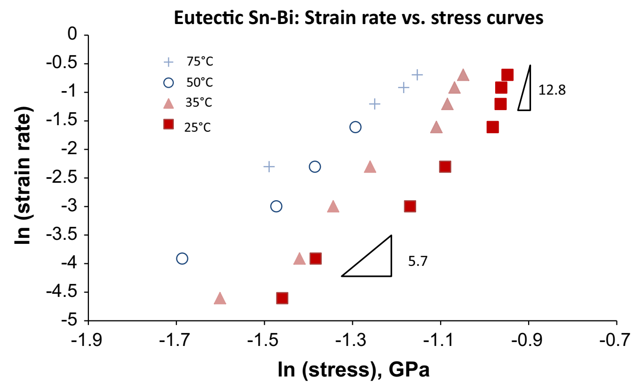

Fig. 9 Strain rate–stress curves for eutectic Sn–Bi measured at different temperatures

(0.01–0.2 s^{-1}) throughout the whole temperature range being tested.

To understand the creep mechanism in this alloy, the results are re-plotted in the form of ln(σ) versus (*1/T*), as shown in Fig. 10. The curves display different slopes when the strain rate changes. However, they could typically be grouped into two ranges. At high strain rates (0.3–0.5 s^{-1}), the curves have a lower slope with an average value of 453.1 K; while at lower strain rates (0.02–0.2 s^{-1}), the curves have a higher slope with an average value of 1168.5 K. The calculation of the activation energy of eutectic Sn–Bi is thus separated according to strain rates and temperatures:

At high strain rates (0.3–0.5 s^{-1}) and low temperature (25–35 °C):

$$Q_1 = 12.8 * R * 453.1 = 48.2\,\mathrm{kJ/mol}$$

At low strain rates (0.02–0.2 s^{-1}) and high temperature (50–75 °C):

$$Q_2 = 5.7 * R * 1168.5 = 55.6\,\mathrm{kJ/mol}$$

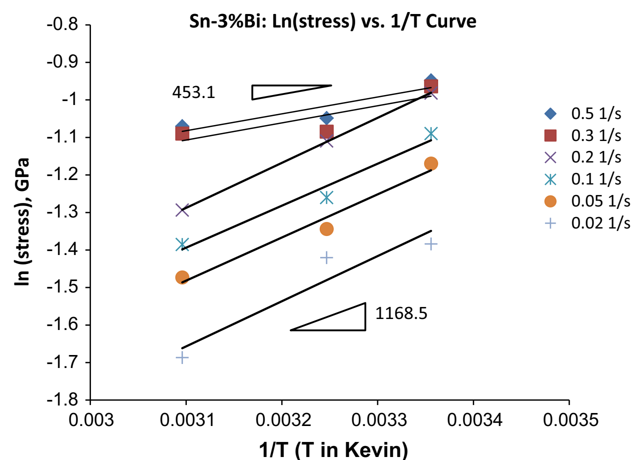

Fig. 10 Ln(stress) versus (1/T) curves for Sn–3%Bi

It is noticed that in spite of the distinct different stress exponents obtained at different strain rates, close activation energies are obtained for the eutectic Sn–Bi alloy. Table 4 summarises the average stress exponents (n) and creep activation energies (Q) for Sn, Bi, Sn–3%Bi solid solution and eutectic Sn–Bi alloy measured from current study. Assigning the creep mechanism for eutectic Sn–Bi alloy is not straight forward as there are two constituent phases involved in the deformation. Raeder et al. [1] has reported two stress exponents appeared in Sn–Bi alloy when it is stressed at different ranges. They attributed the dual-stress response behaviour to the changeover of load bearing phase. The critical stress is approximately 3 MPa, below which Bi is the load bearing phase; while above which Sn-rich phase is the one sustaining the stress. If this is the case, the creep rates at different stress ranges should follow the ones of the dominant phase at the corresponding stress range.

From our study, at higher strain rate (0.3–0.5 s^{-1}) and low temperature (25–35 °C) regime, the creep exponent of eutectic Sn–Bi is found to be close to that of the Sn–3%Bi solid solution (Table 4) implying the creep rate of the two-phase alloy could be controlled by the atomic movement inside this phase. As suggested by Raeder et al. [1], at higher stress region, Sn-rich phase is the main load bearing phase at high strain rate region. The low activation energy (48.2 kJ/mol) found in the alloy could be attributed to the lower T_m of the eutectic Sn–Bi alloy. The activation energy needed to prompt the same creep rate in this alloy is less than that for the high melting point Sn–3%Bi. As the high creep exponent and relatively low activation energy correspond well with the characteristics of *Low Temperature Creep* behaviour, the creep rate of the alloy is believed to be limited by dislocation climb by core diffusion in the Sn-rich phase.

In the lower strain rate (2×10^{-3}–0.2 s^{-1}) regime, the creep stress exponent of eutectic Sn–Bi alloy is found to be 5.7 implying a power-law creep in operation in this testing condition. Lower stress exponent than any of the constituent phase materials implies the rate of creep in the two-phase alloy is not solely controlled by any one of the constituent phases. The activation energy of 55.6 kJ/mol corresponds to the *Low Temperature Creep* behaviour, with both constituent phases participate in deformation.

5 Discussion

5.1 Nanoindentation creep and bulk creep tests

Nanoindentaiton creep test is relatively simple and fast test method compared to the conventional creep test using a bulk sample. However, caution should be made when comparing the data obtained between the two test methods. The number of grains surveyed by nanoindentation is much smaller than the one by conventional bulk creep test. When the grain size is large, the properties measured are dependent on the orientation of the grains that are indented. The problem becomes more complicated with Sn, which displays strong anisotropic behaviour. Among the four types of samples tested in the current work, pure Sn and pure Bi have much larger grain size (average grain size are 317 and 111 µm respectively) than the indentation mark (edge of the triangle is around 28 µm), five grains for each test condition is insufficient to represent the bulk sample data. On the other hand, the Sn–3%Bi (single phase) and eutectic Sn–Bi (two phase) samples have an average grain size of 9 µm and inter-phase space of 2.6–2.7 µm, respectively. One indent covers several grains in these two samples. The averaged creep data are therefore more valid to be used to compare with the bulk creep test data.

Nevertheless, the value of the obtained data of pure Sn and pure Bi should not be completely denied or underestimated. Nanoindentaiton is the only technique to directly assess materials properties of a small volume, such as solder joints encountered in modern electronic devices. In flip chip packages, solder balls of the size in the range of 50–100 µm are typically encountered. In such a case, each solder joint consists of very few crystal grains. Nanoindentation technique is able to provide valuable creep data of the actual solder materials in a device. Using conventional bulk creep samples in this case becomes inferior and less valid compared to nanoindentation test.

5.2 Thermal drift

The causes of indentation thermal drift mainly come from two sources: (1) the heat generated during the experiment from the interferometric displacement assembly mounted close to the indenter on the indenter shaft, and (2) the environmental temperature change due to the instability of the externally controlled temperature stage. To address first drift cause, the manufacturer of the nanoindenter has improved the configuration of the displacement assembly to be further apart from the indenter without compromising the accuracy of the measurement comparing to the previous models. The thermal drift from this source has shown to be negligible with the lasted few models [18]. On the controlling of the sample temperature, the specimen was in close contact with the samples stage at the experiment temperature for at least 30 min prior to the indentation penetration starts. However, it is still a challenge to minimize the temperature fluctuation introduced at the initial contact of indenter and the material. With the effort of

minimizing the thermal drift effect, e.g., using relatively large indentation depth and loading within a relative short period of time as suggested by Wheeler [25], the impact to measurements is expected to be expected to be reduced to a minimum.

6 Conclusions

In this study, indentation CSR testing protocol has been established and used to determine the creep stress exponent and the activation energy of Sn, Bi and their alloys with one or two constituent phases. The creep mechanism of the two-phase eutectic Sn–Bi alloy has been thoroughly discussed with the contributions from its constituent phases. The limitation and usefulness of nanoindentaiton creep data have been discussed.

The activation energy and stress exponent of pure Sn are found to be 48.8 kJ/mol and 8.9 through the high temperature CSR indentation tests. Dislocation climb controlled by core diffusion in bulk is suggested to be the deformation mechanism in Sn samples (with grain size larger than 100 μm).

Creep mechanisms of pure Bi and Sn–3%Bi are suggested to be dislocation climb through core diffusion and PLB, respectively. GBS serves as a complementary mechanism to accommodate grain shape change from the PLB deformation in Sn–3%Bi solid solution.

The creep rate of eutectic Sn–Bi under higher strain rates (0.3–0.5 s^{-1}) and low temperature (25–35 °C) regime is controlled by dislocation climb in Sn-rich phase through core diffusion. The stress exponent and activation energy are found to be 12.8 and 48.2 kJ/mol, respectively. At lower strain rate region (2×10^{-3}–0.2 s^{-1}), the stress exponent of 5.7 and activation energy of 55.6 kJ/mol suggest that the creep rate of eutectic Sn–Bi alloy is controlled by dislocation climb in both constituent phases.

References

1. C.H. Raeder, D. Mitlin, R.W. Messler Jr., Modelling the creep rates of eutectic Bi–Sn solder using the data from its constitutive phases. J. Mater. Sci. **33**, 4503–4508 (1998)
2. C.H. Raeder, G.D. Schmeelk, D. Mitlin, T. Barbieri, W. Yang, L.F. Felton, R.W. Messler, D.B. Knorr, D. Lee, Isothermal Creep of Eutectic SnBi and SnAg Solder and Solder Joints, in *Sixteenth IEEE/CPMT International Electronics Manufacturing Technology Symposium* (1994), pp. 1–6
3. M.D. Mathew, H. Yang, S. Movva, K.L. Murty, Creep deformation characteristics of tin and tin-based electronic solder alloys. Metall. Mater. Trans. A **36A**, 99–105 (2005)
4. J.L.F. Goldstein, J.W. Morris, Microstructural development of eutectic Bi–Sn and eutectic In–Sn during high-temperature deformation. J. Electron. Mater. **23**, 477–486 (1994)
5. Z. Mei, J.W. Morris Jr., Characterization of eutectic Sn–Bi solder joints. J. Electron. Mater. **21**, 599–607 (1992)
6. D. Mitlin, C.H. Raeder, R.W. Messler Jr., Solid solution creep behavior of Sn–xBi alloys. Metall. Mater. Trans. A **30A**, 115–122 (1999)
7. X.Q. Shi, Z.P. Wang, Q.J. Yang, H.L.J. Pang, Creep behavior and deformation mechanism map of Sn–Pb eutectic solder alloy. J. Eng. Mater. Technol. Trans. ASME **125**, 81–88 (2003)
8. M.M. El-Bahay, M.E. El Mossalamy, M. Mahdy, A.A. Bahgat, Some mechanical properties of Sn–3.5 Ag eutectic alloy at different temperatures. J. Mater. Sci.: Mater. Electron. **15**, 519–526 (2004)
9. V.M.F. Marques, B. Wunderle, C. Johnston, P.S. Grant, Nanomechanical characterization of Sn–Ag–Cu/Cu joints—part 2: nanoindentation creep and its relationship with uniaxial creep as a function of temperature. Acta Mater. **61**, 2471–2480 (2013)
10. H.L. Reynolds, *Creep of two-phase microstructure for microelectronic applications* (Department of Materials Science and Mineral Engineering, University of California, Berkeley, 1998), p. 98
11. J.W. Morris Jr., J.L.F. Goldstein, Z. Mei, Microstructure and mechanical-properties of Sn–In and Sn–Bi solders. JOM **45**, 25–27 (1993)
12. T. Reinikainen, J. Kivilahti, Deformation behavior of dilute SnBi(O.5 to 6 At. Pct) solid solutions. Metall. Mater. Trans. A **30**, 123–132 (1999)
13. L. Shen, W.C.D. Cheong, Y.L. Foo, Z. Cheng, Nanoindentation creep of tin and aluminium: a comparative study between constant load and constant strain rate methods. Mater. Sci. Eng. A **532**, 505–510 (2012)
14. L. Shen, P. Lu, S. Wang, Z. Chen, Creep behaviour of eutectic SnBi alloy and its constituent phases using nanoindentation technique. J. Alloys Compd. **574**, 98–103 (2013)
15. L. Shen, P. Septiwerdani, Z. Chen, Elastic modulus, hardness and creep performance of SnBi alloys using nanoindentation. Mater. Sci. Eng. A **558**, 253–258 (2012)
16. L. Shen, Z.Y. Tan, Z. Chen, Nanoindentation study on the creep resistance of SnBi solder alloy with reactive nano-metallic fillers. Mater. Sci. Eng. A **561**, 232–238 (2013)
17. J. Dean, A. Bradbury, G. Aldrich-Smith, T.W. Clyne, A procedure for extracting primary and secondary creep parameters from nanoindentation data. Mech. Mater. **65**, 124–134 (2013)
18. B.N. Lucas, W.C. Oliver, Indentation power-law creep of high-purity indium. Metall. Mater. Trans. A **30**, 601–610 (1999)
19. M.J. Mayo, R.W. Siegel, A. Narayanasamy, W.D. Nix, Mechanical-properties of nanophase TiO_2 as determined by nanoindentation. J. Mater. Res. **5**, 1073–1082 (1990)
20. S.N.G. Chu, J.C.M. Li, Impression creep of beta-tin single-crystals. Mater. Sci. Eng. **39**, 1–10 (1979)
21. R.E. Frenkel, O.D. Sherby, J.E. Dorn, Activation energies for creep of cadmium, indium, and tin. Acta Metall. **3**, 470–472 (1955)
22. S. Otake, Y. Ishii, N. Matsuno, Migration energy of vacancies in bismuth. Jpn. J. Appl. Phys. **20**, 1037–1040 (1981)
23. H.J. Frost, M.F. Ashby, *Deformation-mechanism maps: the plasticity and creep of metals and ceramics* (Pergamon Press, New York, 1982)
24. H.J. Frost, M.F. Ashby, Web source from Thayer School of Engineering at Dartmouth. Deformation-mechanism maps: the plasticity and creep of metals and ceramics. http://engineering.dartmouth.edu/defmech/

25. J.M. Wheeler, D.E.J. Armstrong, W. Heinz, R. Schwaiger, High temperature nanoindentation: the state of the art and future challenges. Curr. Opin. Solid State Mater. Sci. **19**, 354–366 (2015)
26. V. Raman, R. Berriche, An investigation of the creep processes in tin and aluminum using a depth-sensing indentation technique. J. Mater. Res. **7**, 627–638 (1992)
27. M.J. Mayo, W.D. Nix, A micro-indentation study of superplasticity in Pb, Sn, and Sn–38 wt%-Pb. Acta Metall. **36**, 2183–2192 (1988)
28. E.A. Brandes, G.B. Brook, *Smithells Metals Reference Book* (Elsevier Butterworth-Heinemann, London, 1988)